HIERARCHICAL SEGMENTATION OF MULTIPLE SCLEROSIS LESIONS IN MULTI-SEQUENCE MRI

G. Dugas-Phocion[1], *M.A. González*[1], *C. Lebrun*[2], *S. Chanalet*[2], *C. Bensa*[2], *G. Malandain*[1], *N. Ayache*[1]

[1]INRIA, Projet Epidaure, 2004 Route des Lucioles BP 93, Sophia Antipolis, 06902 France
[2]CHU Pasteur, Service de Neurologie, 30 voie romaine BP 69, Nice, 06002 France

ABSTRACT

Automatic segmentation of multiple sclerosis lesions in magnetic resonance images remains a challenging task. In this study, we present a fully automatic method to extract lesions from multi-sequence MRI (T1, T2, T2 FLAIR, Proton Density) within an EM based probabilistic framework. The method uses the available MRI sequences in a hierarchical, orderly manner. First the T2 FLAIR sequence is used to generate a segmentation of supra-tentorial lesions. Then T2 and T1 lesion loads are computed, providing an insight into lesion structure. A priori anatomical knowledge is incorporated in the form of a probabilistic brain atlas.

1. INTRODUCTION

Magnetic Resonance Imaging (MRI) is the primary complementary exam for the monitoring and diagnosis of multiple sclerosis (MS) [1]. MS lesions exhibit hypersignals in T2 and hyposignals in T1, with respect to normal white matter intensities. Typically, lesions appear smaller in T1 than T2, reflecting their complex internal structure. T1 lesion load has already been successfully correlated with the Expanded Disability Status Scale (EDSS) using large sets of patients, while there is little evidence of the clinical relevance of T2 lesion load [2]. In any case, an automatic segmentation system that generates different quantifiers is useful for diagnosis and clinical trials [3].

Hyperintense signals in T2 images provide a good measure of the overall tissue injury [4]. However, since the intensities of lesions and cerebro-spinal fluid (CSF) are close, this may lead to misclassification. The T2 FLAIR sequence offers good contrast between MS lesions and CSF [5]. Even though it highlights supra-tentorial lesions mostly, it is known that using this sequence increases sensitivity and specificity for the case of MS lesion segmentation [6].

Existing multi-sequence MS lesion segmentation methods [7, 8, 9] give equal importance to the set of MRI sequences, which are employed all at once, ignoring their differences. Instead, we propose a hierarchical method that uses information in an orderly manner. We first consider the four sequences – T1, T2, T2 FLAIR, Proton Density – to build a mask of brain tissues, and segment them into three classes : white matter, grey matter, CSF. The parameters are then extracted to automatically compute a threshold that we apply on the T2 FLAIR sequence to get a mask of MS lesions. Finally, we can separate outliers from lesions and use this mask to aid in the segmentation of T1 data and the computation of lesion loads.

2. BRAIN TISSUE SEGMENTATION

The image database consists of 27 patients, each one containing 4 sequences: T1, T2, T2 FLAIR, Proton Density. We apply an intra-patient rigid registration of all sequences so that a voxel represents the same point in the four images. To this end, we employ our iconic block-matching based robust registration algorithm, implemented in a fully-automatic program that performs the registration within the range of the minute [10]. A statistical prior for healthy tissue will be used in our probabilistic segmentation framework, namely the Brainweb atlas from Montreal Neurological Institute [11]. An affine registration of this atlas to each dataset is computed, again using [10].

2.1. Brain Mask Extraction

In order to detect white matter lesions, we first separate skull and fat from brain tissues. Our method is described next; alternative techniques can be found in [12].

The MRI intensity signature of brain tissues shows some dispersion due to normal anatomical variability: as an example, the corpus callosum is known to be brighter than hemispheric white matter in T2 images. These variations are minor though, and considering three classes among brain tissues is reasonable. MRI noise is known to follow a Rician density, which can be fairly approximated by a Gaussian distribution. We use an Expectation Maximization (EM) algorithm [13] to compute the segmentation: we extract seven classes from the four sequences, three of them being brain tissues: white matter, grey matter, CSF.

The EM algorithm consists in iterating two steps: fuzzy labelization of the image (Expectation step) and estimation

of the class parameters by maximizing the likelihood of the whole image (Maximization step).

The labelization is the computation of the probability of a tissue class given the image and the parameters. The application of Bayes' rule gives the solution of the problem, summarized in equation 1. l_j and y_j are respectively the label and the multi-spectral intensity of the voxel j ; Y is the whole image and Φ is the set of parameters. π_{l_j} is the *a priori* probability to get a label for the voxel j.

$$p(l_j|Y,\Phi^{m-1}) = \frac{p(y_j|l_j,\Phi^{(m-1)}) * \pi_{l_j}}{\sum_k p(y_j|l_j=k,\Phi^{(m-1)}) * \pi_{l_j=k}} \quad (1)$$

π_{l_j} is different whether a probabilistic atlas is available or not. When no atlas is used, the prior does not depend on the position j of the voxel and needs to be re-estimated at each iteration. When the atlas is available, the spatially dependent prior simply needs to be normalized so that the sum is equal to 1.

The estimators that maximize the likelihood are the ML estimators corresponding to the mean and covariance matrix. As an approximation, we use the parameters of the last iteration $\Phi^{(m-1)}$ when computing the parameters at iteration m. Both estimators are represented within equations 2 and 3 :

$$\mu_k^m = \frac{\sum_j f(l_j=k|Y,\Phi^{(m-1)}) * y_j}{\sum_j f(l_j=k|Y,\Phi^{(m-1)})} \quad (2)$$

$$\Sigma_k^m = \frac{\sum_j f(l_j=k|Y,\Phi^{(m-1)}) * (y_j-\mu_k^m)(y_j-\mu_k^m)'}{\sum_j f(l_j=k|Y,\Phi^{(m-1)})} \quad (3)$$

Using the labelization of the brain tissues and mathematical morphology, we extract a brain mask (Figure 1). In some rare cases, the system fails to separate the eyes from the brain. However, such problems can be detected using the atlas, so the method remains automatic.

2.2. Healthy Brain Tissue Segmentation

The labelization and parameters of the three brain tissue classes extracted from the algorithm above cannot be directly used as brain tissue segmentation: since there is no spatial prior, some voxels within the skull and fat are misclassified. Furthermore, lesions within the segmentation will be labeled as CSF or grey matter, which will alter the computation of class parameters. That is the reason why the segmentation of grey matter, white matter and CSF needs to be computed again, but only within the previously extracted brain mask.

Each class is still defined by a set of parameters – mean and covariance matrix – and a fuzzy labelization that corresponds to the probability of each voxel to belong to the class. The algorithm consists in iterating three steps: estimate the labelization, compute the parameters by maximizing the likelihood of the overall image and estimate outliers.

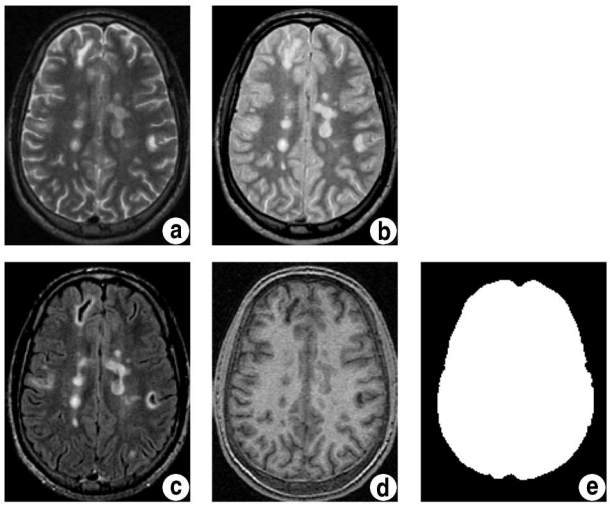

Fig. 1. Input MRI : a) T2, b) Proton Density, c) T2 FLAIR, d) T1 and e) the EM-generated brain mask.

The main difference between this algorithm and that used to extract the mask is the addressing of outliers. In the third step, potential outliers are detected and eliminated. This detection is derived from the computation of the parameters during the Maximization step. The Mahalanobis distance between each voxel intensity and each class is computed in equation 4. If the distance is greater than a threshold for the three classes, the corresponding voxel is labeled as an outlier: it will not be used for the next step to estimate the parameters.

$$d_{j,k} = (y_j-\mu_k^m)'(\Sigma_k^m)^{-1}(y_j-\mu_k^m) \quad (4)$$

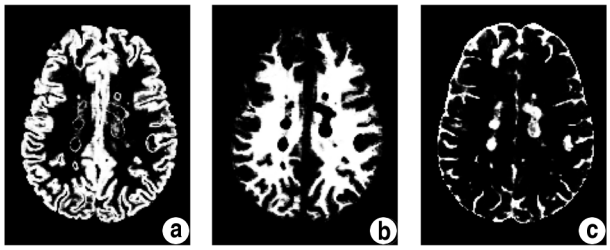

Fig. 2. Representation of the probability to belong to each class : a) grey matter, b) white matter, c) CSF. While most lesions are labeled as CSF, some of them are labeled as grey matter.

The process of classifying the tissues takes less than a

minute on a regular computer, and results are shown in figure 2. Notice that the fuzzy segmentations are probability maps corresponding to the three classes for each voxel, even the ones marked as outliers. The latter voxels are labeled as the best class possible, which is usually CSF for intense lesions, or grey matter for low-contrast lesions.

3. T2 FLAIR LESION EXTRACTION

Tissue parameters (mean and covariance matrix) for each tissue class have been computed above. Since T2 FLAIR offers a good contrast between lesions and CSF, and since hyperintense signals represent the globality of the lesion, we are only using this sequence to extract a primary lesion mask. This segmentation in a single sequence becomes a Mahalanobis threshold, which is computed from the class parameters restricted to the T2 FLAIR sequence. Since the number of dimensions has been reduced, the Mahalanobis threshold needs to be adjusted according to the χ^2 rule. This is why the threshold is not a simple projection on the T2 FLAIR axis (Figure 3).

We therefore compute the 1D-Mahalanobis distance to the three classes, and take the upper threshold to separate lesions from healthy tissues. The obtained threshold is independent of the intensity range of original images, since the Mahalanobis distance acts like a intensity normalization process. This method shows good results, as presented in Figure 5.

n	$k_{\gamma=0.50}$	$k_{\gamma=0.90}$	$k_{\gamma=0.99}$	$k_{\gamma=0.999}$
1	0.67449	1.64485	2.5783	3.29053
2	1.17741	2.14597	3.03485	3.71692
3	1.53817	2.50028	3.36821	4.03314
4	1.83213	2.78916	3.64372	4.29730

Fig. 3. Table giving the threshold over which, following the χ^2 rule, a point will be labeled as an outlier. The number of dimensions n is known, and so is the probability of false positive $1-\gamma$. We set γ to 0.90, which means there is a 10% error to get a false positive. This corresponds to a Mahalanobis threshold of 2.74 using the four sequences, and 1.64 using only the T2 FLAIR sequence

A very sensitive Mahalanobis threshold was chosen, so that no lesions were missed. Therefore, some of the labeled voxels may be outliers, rather than true lesions. We have included two different steps to differentiate the two. First, the white matter atlas is used to check if those points are likely to be located in the white matter; and second, we verify the connectivity between lesions and white matter by clustering the lesions and checking the neighboring voxels. This results in a good mask of lesions which can be used to extract the different lesion loads (Figure 5.c).

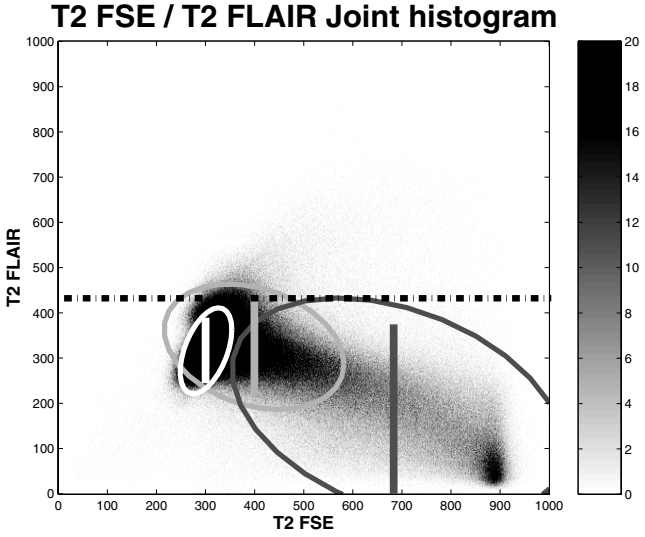

Fig. 4. T2 / T2 FLAIR joint histogram. The three ellipses represent the iso-distance curve to each class : white matter (white), grey matter (light grey), CSF (dark grey). The corresponding segment within each ellipse represents the confidence interval for each class, with respect to the T2 FLAIR sequence. The upper threshold is shown as a dot-dashed line: the lesions are points over it.

Now that a first lesion mask has been computed, we proceed to compute the quantifiers that have a well-known clinical meaning, namely lesion loads. The T2 FLAIR load can be computed directly from the mask: it is the volume of the voxels labeled as lesions.

4. COMPUTATION OF T1 LESION LOAD

The T1 load is computed next. T1 lesions are hyposignals within the white matter, and they are a subset of T2 lesions. Differences between T2 and T1 segmentations for a given lesion can provide useful information about the structure of the lesion. To extract T1 lesions, a two class EM on the T1 voxels corresponding to the previously obtained T2 lesion mask is performed. The parameters are initialized to the ones of white matter for the first class, and we simply half the mean to initialize the second class, which will contain T1 lesions. The resulting probabilities are thresholded to obtain a binary classification, and T1 load is computed in a similar way as for T2 (Figure 5.e,f).

5. CONCLUSION AND FUTURE WORK

We presented a novel MS lesion segmentation algorithm that employs multi-sequence information in an orderly manner. Thanks to contrast in the T2 FLAIR sequence, the sys-

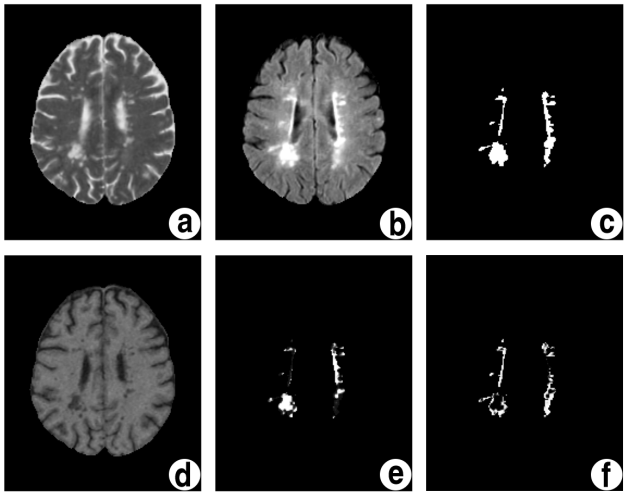

Fig. 5. Final results : a) T2, b) T2 FLAIR, c) resulting mask of T2 FLAIR lesions, d) T1, e) corresponding T1 lesion mask, and f) T1/T2 difference map.

tem does not miss small juxta-cortical lesions that are useful for diagnosis. T1 lesion segmentation is accurate, because the T2 FLAIR lesion mask acts as a powerful denoising tool. Computation time, including registration, is in the order of a few minutes, which will make the technique usable as a diagnosis help tool.

Future work focuses on on-going validation studies, the incorporation of knowledge particular to the physics of the MRI sequences employed, the analysis of partial volume effects to obtain sub-voxel accuracy [14] and the interpretation of the T1/T2 difference map as a tool for lesion characterization.

6. REFERENCES

[1] A. Tourbah, "IRM et sclérose en plaques," *Neurologies*, vol. 4, no. 33, pp. 270–274, 2001.

[2] J. Grimaud, Y.-M. Zhu, and M. Rombaut, "Mise au point : Les techniques d'analyse quantitative des IRM cérébrales : application à la sclérose en plaque," *Revue Neurologique*, vol. 158, no. 3, pp. 381–389, 2002.

[3] E.M. Frohman, D.S. Goodin, P.A. Calabresi, J.R. Corboy, P.K. Coyle, M Filippi, J.A. Frank, S.L. Galetta, R.I. Grossman, K. Hawker, N.J. Kachuck, M.C. Levin, J.T. Phillips, M.K. Racke, V.M. Rivera, and W.H. Stuart, "The utility of MRI in suspected MS: Report of the Therapeutics and Technology Assessment Subcommittee of the American Academy of Neurology," *Neurology*, vol. 61, no. 5, pp. 602–11, 2003.

[4] M. Filippi and R.I. Grossman, "MRI techniques to monitor MS evolution : the present and the future," *Neurology*, vol. 58, no. 8, pp. 1147–1153, 2002.

[5] I.L. Tan, R.A. van Schijndel, P.J. Pouwels, H.J. Ader, and F. Barkhof, "Serial isotropic three-dimensional fast FLAIR imaging: using image registration and subtraction to reveal active multiple sclerosis lesions," *AJR Am J Roentgenol*, vol. 179, no. 3, pp. 777–82, 2002.

[6] E.H. Herskovits, R. Itoh, and E.R. Melhem, "Accuracy for detection of simulated lesions: comparison of fluid-attenuated inversion-recovery, proton density–weighted, and T2-weighted synthetic brain MR imaging," *AJR Am J Roentgenol*, vol. 176, no. 5, pp. 1313–8, 2001.

[7] K. Van Leemput, F. Maes, D. Vandermeulen, A. Colchester, and P. Suetens, "Automated segmentation of multiple sclerosis lesions by model outlier detection," *IEEE TMI*, vol. 20, no. 8, pp. 677–688, 2001.

[8] M. Kamber, R. Shinghal, D.L. Collins, G.S. Francis, and A.C. Evans, "Model-based 3D segmentation of multiple sclerosis lesions in magnetic resonance images," *IEEE TMI*, vol. 14, no. 3, pp. 442–453, 1995.

[9] B. Johnston, M.S. Atkins, B. Mackiewich, and M. Anderson, "Segmentation of multiple sclerosis lesions in intensity corrected multispectral MRI," *IEEE TMI*, vol. 15, no. 2, pp. 154–169, 1996.

[10] S. Ourselin, A. Roche, G. Subsol, X. Pennec, and N. Ayache, "Reconstructing a 3D structure from serial histological sections," *Image and Vision Computing*, vol. 19, no. 1-2, pp. 25–31, Jan. 2001.

[11] D.L. Collins, A.P. Zijdenbos, V. Kollokian, J.G. Sled, N.J. Kabani, C.J. Holmes, and A.C. Evans, "Design and construction of a realistic digital brain phantom," *IEEE TMI*, vol. 17, no. 3, pp. 463–8, 1998.

[12] M.E. Brummer, R.M. Mersereau, R.L. Eisner, and R.R.J. Lewine, "Automatic detection of brain contours in MRI data sets," *IEEE TMI*, vol. 12, no. 2, pp. 153–166, 1993.

[13] A. Dempster, N. Laird, and D. Rubin, "Maximum likelihood from incomplete data via the EM algorithm," *Journal of the Royal Statistical Society*, vol. 39, no. 1, pp. 1–38, 1977.

[14] M.A. González Ballester, A. Zisserman, and M. Brady, "Estimation of the partial volume effect in MRI," *Medical Image Analysis*, vol. 6, no. 4, pp. 389–405, 2002.